WILEY-VCH

DOI: 10.1002/ ((please add manuscript number))
Article type: Full paper

Photophysical study of DPPTT-T/$PC_{70}BM$ blends and solar devices as a function of fullerene loading: an insight into EQE limitations of DPP-based polymers.

*Elisa Collado-Fregoso, Florent Deledalle, Hendrik Utzat, Pabitra S. Tuladhar, Stoichko D. Dimitrov, Alexander Gillett, Ching-Hong Tan, Weimin Zhang, Iain McCulloch and James R. Durrant**

Dr. E. C.-F. Author 1, Dr. F. D. Author 2, H.U. Author 3, Dr. P.S.T. Author 4, Dr. S.D.D. Author 5, A.G. Author 6, C.-H.T. Author 7, W.Z. Author 8, Prof. I.M. Author 9, Prof. J.R.D Author 10
Centre for Plastic Electronics, Department of Chemistry, Imperial College London, Exhibition Road, London SW7 2AZ, United Kingdom
E-mail: j.durrant@imperial.ac.uk
H.U. Author 3
Department of Chemistry, MIT, 77 Massachusetts Ave. Room 2-216 Cambridge, MA 02139 USA
A.G. Author 6
Cavendish Laboratory, Department of Physics, University of Cambridge, J J Thomson Ave., Cambridge CB3 0HE, United Kingdom
Prof. I.M. Author 9
SPERC, King Abdullah University of Science and Technology, Thuwal 23955-6900, Saudi Arabia
Prof. J.R.D Author 10
SPECIFIC IKC, College of Engineering, Swansea University, SA12 7AX, U.K.

Keywords: organic photovoltaics, DPP-based solar cells, donor-acceptor composition, EQE limitations

Abstract: Diketopyrrolopyrrole (DPP)-based polymers have been consistently used for the fabrication of solar cell devices and transistors, due to their high crystallinities resulting in high electron and hole mobilities. However, they also often show limited external quantum efficiencies (EQEs). In this contribution we analyze the limitations on EQE by a combined study of exciton dissociation efficiency, charge separation and recombination kinetics in thin films and solar devices of a DPP-based donor polymer, DPPTT-T blended with varying weight fractions of the fullerene acceptor $PC_{70}BM$. From the correlations between photoluminescence quenching (PLQ), transient absorption studies and EQE measurements, we conclude that the main limitation of photon-to-charge conversion in DPPTT-T/$PC_{70}BM$

devices is poor exciton dissociation. This exciton quenching limit is related to the low affinity/miscibility of the materials, as confirmed by X-ray diffraction and transmission electron microscopy data, but also to the relatively short DPPTT-T singlet exciton lifetime possibly associated with high non-radiative losses. A further strategy to improve EQE in this class of polymers without sacrificing the good extraction properties in optimized blends is therefore to limit those non-radiative decay processes.

1. Introduction

Diketopyrrolopyrrole (DPP)-based polymers have been widely studied as donor components in organic photovoltaic devices.[1–19] Their donor-acceptor design, with an electron deficient DPP core and electron rich thiophenes, results in a narrow bandgap, capable of absorbing photons in the near-IR region. Their low bandgaps make them suitable to be used as the low-wavelength co-absorbing material in tandem solar cells.[4,8,15] It has been shown that they can constitute single junction devices as blends with fullerene acceptors yielding close to 9% power conversion efficiencies (PCE).[8,15] Moreover, they can present high and balanced charge carrier mobilities, a feature that confers them ambipolar characteristics interesting for applications in organic transistors.[5,8,10,11,14,15] They also exhibit remarkably strong visible absorptivities, which has been related to their long structural persistence lengths.[20] However, a common problem present in the majority of DPP-based organic photovoltaic (OPV) devices is that, despite having good fill factors (*FF*), open circuit voltage (V_{OC}), and light harvesting properties, their external quantum efficiencies (*EQE*s) are relative modest, limiting their short circuit currents (J_{SC}) performance. In this paper, we focus on the origin of this EQE limitation for DPP-based organic solar cells.

Evidence that DPP-based organic solar cells indeed are particularly limited by modest *EQE* values is presented in **Table 1**. This table shows an analysis of performance figures from recent literature of the best single-junction DPP-based conventional devices versus the best

analagous devices employing non-DPP based donor polymers. The DPP-based devices exhibit lower bandgaps than most efficient non-DPP based devices, and therefore should be able to harvest a larger fraction of the solar spectrum. However their average J_{SC} values are similar to those of non-DPP devices, explained by the DPP-devices exhibiting lower EQE values. These lower EQEs values are observed both in the blue part of the spectrum, associated with fullerene charge generation and in the red, polymer-charge generation wavelengths, but they are particularly noticeable in the latter case. While the maximum EQE for DPP systems has an average value of 57%, the same figure for non-DPP devices averages 75%. We rule out systematic absorption strength limitations in the DPP-based devices since their active blend thickness are similar or even thicker than those of the non-DPP based devices. Moreover, there is no evidence suggesting that DPP-based polymers have lower extinction coefficients compared to their non-DPP based counterparts; quite the opposite, recent studies suggest that at least DPPTT-T presents a considerably higher extinction coefficient compared to other polymers used for photovoltaic devices.[20] Therefore, these lower EQE figures appear related to the intrinsic ability of these polymers to convert photons into photocurrent.

The data in Table 1 suggests that despite DPP-based capability of harvesting low-energy photons which contribute to J_{SC}, they have an intrinsic conversion limitation that lowers their EQE values. A few studies have recently addressed EQE limitations in DPP-based polymers. One of these studies used DPP polymers with different donor moieties,[4] another one studied P-DPPTPT with varying side chains.[7] Both works found that the optimized blends form fibrillar microstructures whose widths were inversely correlated with EQE values. The study with P-DPPTPT proposed that wide polymer fibrillar structures prevent an efficient exciton dissociation which impacts upon the EQE values for the corresponding devices. Yet another publication[17] uses a set of five polymers with increasing relative amounts of Selenophene-substituted copolymer to increase the polymer crystallinity. The study shows that despite

highly crystalline DPP based polymers having high charge mobilities, they also result in a drop in the PCE for the associated photovoltaic devices, related to unfavorable morphology with extensive phase separation.

The study herein presented investigates the relationship between exciton dissociation, charge separation and charge recombination in blend films and devices fabricated with DPPTT-T, a highly crystalline polymer that has been used to fabricate solar devices with very high J_{SC} but relatively modest EQE (see Table 1). We control blend morphologies by varying the $PC_{70}BM$ loadings, and relate the results to the corresponding device characteristics. By a combination of steady-state and transient optical and optoelectronic techniques, we determine the kinetics of charge generation and recombination as well as the effective device mobilities. Morphology and crystallinity characterization including Transmission electron microscopy (TEM), Atomic Force Microscopy (AFM) and Wide angle XRD were used to assess film microstructure upon fullerene addition. Inefficient exciton dissociation on both polymer and fullerene domains is shown to impact directly on the EQE of the corresponding devices, thus explaining the low-EQEs despite the high J_{SC} in optimal devices. A comparison with other DPP-based devices and regioregular-P3HT suggest that this may be a general trend for devices prepared with crystalline donor polymers with low fullerene miscibilities.

2. Results

2.1. Steady state UV-vis, Photoluminescence emission and morphological assays.

2.1.1. UV-visible and Photoluminescence emission

Figure 1 shows typical steady-state UV-vis absorption spectra of neat DPPTT-T and $PC_{70}BM$ films as well as of DPPTT-T:$PC_{70}BM$ blends as a function of their weight ratio, varying from 4:1 to 1:10 polymer:fullerene. As expected, upon increasing the fullerene ratio, the proportion of $PC_{70}BM$ absorption increases, whereas the 650 – 1000 nm polymer absorption decreases.

Interestingly, it is noticeable that upon increasing the $PC_{70}BM$ concentration, the relative intensity of the 0,1 vibronic transition, increases with respect to the lowest 0,0 transition. Additionally, a slight red shift in the $S_0 \rightarrow S_1$ transition of ~ 0.04 eV is also observed (from 793 nm in the neat polymer to 814 nm in the 1:10 blend). These observations have been argued to originate from an increased order in the polymer packing due to increased $\pi - \pi$ stacking,[21,22] resulting from a higher contribution of linear packing in the polymer chains, as determined by Vezie and co-workers using resonance Raman studies.[20] This assignment also agrees with the decrease in the 0,0 vibronic intensity when a DPPTT-T solution in ODCB solvent is heated, (shown in **Figure S1**) and thus the intermolecular polymer interactions disrupted as the polymer chains gain are able to sample curved conformations. This finding is rather surprising and suggests that polymer interchain interactions are enhanced upon fullerene addition.

Next, in **Figure 2a** and **2b**, we present DPPTT-T and $PC_{70}BM$ photoluminescence (PL) emission spectra, and their respective quenching in the blend films of varying compositions. The polymer emission spans from ~ 850 to 1300 nm and that of the fullerene between ~ 650 and 800 nm. As expected, the quenching degree increases as the concentration of the complementary component increases; i.e., the larger the DPPTT-T concentration, the more quenched is $PC_{70}BM$ emission. It is noticeable that whereas the fullerene quenching is complete or close to being complete for the films with high polymer concentration, polymer emission does not reach complete quenching even in the 1:10 film. This finding indicates an asymmetric dissociation between excitons generated in fullerene and polymer domains, most likely associated with the high intermolecular interaction of DPP chains even in diluted solutions.[20] It is particularly striking that in the blend composition giving optimum device efficiencies (1:2 DPPTT-T:$PC_{70}BM$) both DPPTT-T and $PC_{70}BM$ emission quenching are

substantially less than 100%, with values for the PLQ efficiency of 68 and 71 % respectively, as shown in **Table 2**.

In previous studies, the degree of PL quenching has been related to the degree of intermixing, that is the length scale of phase segregation, estimated as the average distance *L* that the exciton can travel before encountering a polymer/fullerene interface.[23,24] A key parameter needed to estimate *L* is the neat material exciton diffusion length L_{ex}. We estimated this distance by using an analysis similar to that described in ref.[25] of exciton transient absorption decay data at different excitation fluencies, detailed in Section 2 of the Supporting Information (SI). From the analysis, we obtained a polymer exciton diffusion length ≤ 6 nm. This is a relatively small diffusion length compared to other conjugated polymers[26] and as shown in the next section and the SI, is at least part the result of relatively fast singlet exciton non-radiative decay. For $PC_{70}BM$, the exciton diffusion length we use the reported value of 5 nm.[27,28] We then estimate pure domain diameter as 2*L*, using the PLQ results, as shown in Table 2. Although this approach disregards exciton delocalization, it is a reasonable indication of the level of molecular intermixing present within a blend and therefore, the domain size at the molecular level. Values of the average polymer and $PC_{70}BM$ pure domain diameter determined from this PLQ analysis are listed in Table 2.

2.1.2. Transmission electron microscopy (TEM), and Atomic force microscopy (AFM)

Transmission electron microscopy (TEM) and Atomic force microscopy (AFM) were used to further investigate the morphology of the blend films and compare them to the PLQ data. TEM micrographs for 10:1, 1:1 and 1:4 blends are shown in **Figure 3**(bottom). It appears from the images that upon increasing fullerene concentration, the morphology ranges between essentially undisturbed polymer crystallites in the 10:1 blend, to partial separation of the dark regions assigned to $PC_{70}BM$ domains. Phase separation is observed from the 1:1 blend, and a

notable increase in the size of these domains is observed in the 1:4 blend, similar to that observed by Dimitrov et al.[29] in their BTT-based polymer blends study. Further evidence of domain separation comes from AFM micrographs, (see **Figure S2** in the SI) where the 1:2 blends shows a considerable higher roughness as compared to the 4:1 blend. The observation of fullerene aggregates even in the 1:1 blend is in agreement with the hypothesis that the fullerene solubility within the polymer matrix is low, also observed in the WAXD results discussed below. Values for the fullerene domain diameter sizes from these TEM data are listed in Table 2, and are in reasonable agreement with those estimated from the PLQ results, supporting the validity of our analyses and also suggesting that the fullerene domains are relatively pure.

2.1.3. Wide-angle X-Ray diffraction (WAXD)

Wide-angle X-ray diffraction (WAXD) was used to assess the crystallinity of the blends (both polymer and $PC_{70}BM$ domains) upon increasing $PC_{70}BM$ concentration. Figure 3(top) shows the data obtained for the 4:1, 2:1, 1:2 and 1:4 blend films, corrected to account for the different thicknesses of the blends. A narrow and intense peak can be observed at q = 0.32 $Å^{-1}$, which is in good agreement with the peak obtained for a neat DPPTT-T blend at q = 0.3 $Å^{-1}$.[13,30] This peak has been assigned to out-of-plane lamellar stacking and thus corresponds to a lamellar spacing of 1.96 nm. Importantly, the lamellar spacing does not change for the different blends, inferring that $PC_{70}BM$ does not intercalate strongly between the polymer chains, although some mixing in the amorphous regions of the polymer is expected. The peaks at q = 0.64 and 1.34 $Å^{-1}$ have been previously assigned to fullerene agglomeration.[31,32] A closer analysis to the polymer (lamellar) and fullerene peaks reveals that both peaks intensities correlate linearly with the composition of the blend. That is, the change in the peak intensities for both the polymer and the fullerene can be largely explained by the relative amount of each component. This is shown in **Figure S3** in the SI. In this figure it is also

apparent that the intensity of the lamellar peaks of DPPTT-T in the blends are slightly higher than expected from the decrease in polymer concentration, which agrees with the enhanced linearity observed in the relative intensity of the 0,0 vibronic peak in the steady-state UV-vis spectra, and with the incomplete polymer exciton dissociation in all blends.

2.2. Femtosecond to microsecond transient absorption studies (TAS)

Following the steady-state characterization, transient absorption data was obtained for the films 1:0 (neat DPPTT-T) 4:1, 2:1, 1:2 and 1:4 DPPTT-T:$PC_{70}BM$ after excitation at 740 nm and 25 μJ/cm^2. In order to investigate the asymmetry in the PLQ profiles of the polymer and fullerene, DPPTT-T singlet exciton dynamics was probed at 1000 nm, shown in **Figure 4a** (DPPTT-T neat film transient spectra are shown in **Figure S4a**). As can be observed, the signal has completely decayed by 300 – 400 ps, and can be fitted to a monoexponential decay with a time constant $\tau = 49 \pm 4$ ps. This time is rather short compared to most other exciton decay times in neat conjugated polymers used in OPV studies. As suggested by Dimitrov et al,[26] this may be associated, at least in part, with rapid non-radiative deactivation processes in small bandgap co-polymers such as DPPTT-T, as expected from the energy gap law.[16,33,34] This short exciton lifetime plays an important role in the EQE limitations of DPP-based solar devices, since it requires large intermixing with the fullerene acceptor, as discussed below. As shown in the morphological characterizations, such large intermixing is not the case for DPPTT-T, which forms rather pure, crystallised domains when mixed with $PC_{70}BM$. Simultaneously, it is clear that exciton decay is largely independent of the excitation intensity, at least between 5 and 25 μJ/cm^2, confirming that contributions from exciton annihilation to the overall decays are small , which is also related to the low polymer exciton diffusion length.

It was interesting to draw a correlation between the exciton emission quenching observed in the steady state PLQ measurements of blend films and the early dynamics of the exciton

photoinduced absorption signal at 1300 nm (see typical transient spectra for blends in **Figure S4b** in the SI). At this wavelength the exciton photoinduced absorption dominates the transient signal at early times. **Figure 4b** shows representative exciton photoinduced absorption decay dynamics for the 4:1 and 1:2 blends, where it can be easily observed that the kinetics follow a biphasic decay. The slowest decay times correspond within error to the exciton decay time in neat DPPTT-T films, therefore suggesting that part of the exciton population decays without having met the fullerene acceptor. In this scenario, the fast decay represents the decay of excitons that encounter the interface with $PC_{70}BM$, qualitatively consistent with the steady state PLQ data. To quantify the correlation, the percentage of dissociated excitons, labelled $\%QE$, was calculated as the relative fraction of the pre-exponential factor A_2, associated with the population of quenched excitons, divided by the total population of excitons given by $A_1 + A_2$. The fitting parameters and comparison with steady state PLQ are shown in **Table 3**.

As can be observed in Table 3, $\%QE$ agrees well with the %PLQ obtained by the steady-state measurements, and shows directly the effect of the fullerene "quencher" upon exciton dynamics. The data suggest that photoexcitation of DPPTT-T results in the generation of two distinct populations of DPPTT-T excitons: excitons formed within large DPPTT-T domains which largely decay to ground without generating polarons, and excitons formed in more molecularly mixed (and probably amorphous domains) which are efficiently separated by electron transfer to $PC_{70}BM$ on the ~ 2 ps timescale. The relative proportion of these two exciton populations is modulated by the blend composition, with high $PC_{70}BM$ loading increasing the proportion of DPPTT-T excitons generated in more molecularly mixed regions.

The next section addresses the dynamics of the blend films from the sub-ps to the µs timescale. The films were excited at 5 µJ/cm^2, to assure that the lowest possible energy was used without compromising signal-to-noise ratio. This fluency is equivalent to ~ $5.55 \times$

$10^{16}\ cm^{-3}$, comparable to the charge densities measured in complete devices under solar irradiation. **Figure 5** shows data for the 4:1, 2:1 and 1:2 blend films probing at 980 nm, corresponding to the polaron photoinduced absorption (see Figure S4b in the SI). The transients are normalised for differences in light absorption and exciton quenching between blends, allowing us to consider only the behaviour of polarons following exciton dissociation. It is apparent from this data that the initial polaron signal amplitude is very similar for the blends with different $PC_{70}BM$ loadings, suggesting that the efficiency of polaron (pair) formation per quenched exciton is independent of the relative $PC_{70}BM$ concentration. However, it can be observed that upon increasing the fullerene loading, charge recombination becomes slower, a common observation in a number of studies that have used different transient experimental techniques.[35–40]

In order to determine whether the recombination behaviour observed here corresponds to non-geminate or geminate charge recombination, measurements with different excitation intensities were performed. Representative data is shown in **Figure 6a** for the 4:1 blend and in **Figure 6b** for the 1:4 blend, probing at 980 nm. It is noticeable that upon increasing fullerene loading, the recombination behaviour indeed becomes much slower, going from a polaron half-lifetime of 0.5 ns in the 4:1 blend to 8.8 ns in the 1:4 blend at 1 µJ/cm^2. Moreover, the transients are largely intensity independent in the 4:1 blend but intensity dependent in the 1:4 blend, which suggests a change in the recombination type from geminate to non-geminate. This implies that the relative amount of bound polaron pairs decreases as $PC_{70}BM$ concentration increases, or in other words, that the separation of bound charges into free charges becomes more efficient.

2.3. Solar device characterization and modelling as a function of $PC_{70}BM$ loading: J-V curves, EQE, Transient photovoltage (TPV) and Charge extraction (CE)

Figure 7 shows the J-V curves for devices fabricated with 4:1, 2:1, 1:2 and 1:4 polymer:fullerene blend ratios. The corresponding photovoltaic parameters are presented in **Table 4**. Note that for devices with low fullerene concentrations, both the short circuit current and fill factor are severely limited. It is also evident from Figure 7, that the fill factor of the 1:4 blend is considerably higher than that of the 1:2 blend (see Table 4). This high fill factor most probably results from the greater phase segregation present in the 1:4 blends, which results in slower non-geminate recombination losses, as well as a potential increase in electron mobility.[38] J_{SC} however, is greatly decreased (-30%) when going from the 1:2 to the 1:4 blend, this is in agreement with the 30% decrease in fullerene PLQ, and reduced polymer light absorption. Therefore, it appears that large $PC_{70}BM$ aggregates are necessary to a) avoid extensive geminate recombination, observed in blends with low $PC_{70}BM$ loading and b) slow down non-geminate recombination in all blends. This however happens at the expense of reducing polymer light absorption and losing $PC_{70}BM$ excitons that decay before reaching the interface due to their limited diffusion length, overall resulting in a photocurrent reduction.

We now analyse the optimal, 1:2 DPPTT-T/$PC_{70}BM$ device using charge extraction (CE) and transient photovoltage (TPV) experiments (such data could not be usefully analysed for lower fullerene compositions due to poor charge extraction efficiencies). **Figure 8a** shows the non-geminate recombination rate at different charge densities *n* measured at open-circuit using CE and TPV, as well as the effective mobility measured from our CE determination of *n* at short circuit. From this data, we can estimate a $\mu \cdot \tau$ product between 4.8×10^{-10} and $7.8 \times 10^{-9}\ cm^2V^{-1}$ (at charge densities between 2.2 and $1.1 \times 10^{16}\ cm^{-3}$,respectively) which corresponds to good electrical properties of the device.[41] **Figure 8b** shows the V_{OC} reconstruction for the same 1:2 DPPTT-T/$PC_{70}BM$ device as a function of light intensity. This analysis assumes only non-geminate recombination losses, therefore confirming that *J-V*

curve characteristics are not driven by voltage dependent geminate losses in devices with high fullerene loading, consistent with our fs-TAS studies.

Next, we consider the effect of polymer and fullerene exciton dissociation efficiency (as measured by PLQ data) upon device performance. To estimate the differences in photon to charge conversion per absorbed photon between the different devices, an approximate IQE, EQE/Abs (EQE divided by the number of absorbed photons) is shown in **Figure 9a**. As expected, the highest EQE/Abs was obtained for the best performing 1:2 device, although at long wavelengths (from ~700 nm), the 1:4 device seems to slightly outperform the rest. It is clear from the EQE/Abs normalized at 350 and 780 nm (**Figure S5a** and **S5b**) that devices with higher $PC_{70}BM$ loadings generate photocurrent more efficiently per absorbed photon from polymer absorbing wavelengths, whereas devices with higher polymer loadings, generate photocurrent more efficiently in the $PC_{70}BM$ absorbing wavelengths. This is illustrated in **Figure 9b**, which plots relative PLQ and EQE/Abs as a function of the fullerene fraction (xPCBM). The relative PLQ, in black squares, is calculated as the ratio between $PC_{70}BM$ PLQ and DPPTT-T PLQ; the relative EQE/Abs, in red circles, is calculated as the ratio between the area under the curve for the $PC_{70}BM$ absorbing area in the EQE/Abs graph (considered, as an approximation, from 300 to 560 nm, the left side of EQE/Abs in Figure 9a) and the area under the curve for the polymer absorbing area; (considered from 570 to 850 nm, the right side in Figure 9a). As is apparent in the figure, these two ratios show a clear correlation. This indicates that the differences between the EQE/Abs in the polymer and fullerene absorbing areas can be attributed to the relative polymer and fullerene exciton dissociation efficiencies. It also suggests that incomplete PLQ in the blends has a large impact in current generation in the corresponding devices. However, to take fully into account the effects of geminate recombination, a TPV/CE analysis is necessary for polymer-rich devices.

This was unfortunately precluded due to their poor electrical properties and stability of those devices.

3. Discussion

The study herein presented addresses trends in exciton dissociation, charge separation, recombination and extraction, morphology and device performance for DPPTT-T:$PC_{70}BM$ devices as a function of blend composition. Our study focuses in particular upon losses resulting from inefficient polymer and fullerene exciton quenching, a topic which has received relatively modest attention in the literature.[42,43]

It is worth noting that an argument that could explain incomplete exciton dissociation, even in blends with large fullerene contents, is the small energetic difference in the LUMO levels of DPPTT-T and $PC_{70}BM$ (and therefore driving energies for charge separation, ΔE_{CS}). However, there is some evidence that the morphological effects might be more important. At least three DPP-based polymers similar to DPPTT-T have been used in conventional devices and have reported showing equal or higher EQEs in the polymer area (EQE_{max}^{Pol}) than DPPTT-T/$PC_{70}BM$ devices,[4,7] associated with higher polymer PL quenching. These polymers present lower ΔE_{CS} compared to DPPTT-T, indicating that the low ΔE_{CS} is not a limitation for exciton dissociation.

The impact of polymer crystallinity upon charge recombination losses can be estimated from the extent to which the devices show Langevin-like charge recombination behaviour. While optimal, 1:2 DPPTT-T/$PC_{70}BM$ device presents a non-Langevin reduction factor ζ between 0.02 and 0.18 at charge densities between 1.1 and $2.2 \times 10^{16}\ cm^{-3}$, annealed P3HT devices have reduction factors between 0.002 and 0.0036 at the same charge densities.[44] This represents a ~ 10 fold decrease of the degree of non-Langevin behaviour in DPPTT-T compared to annealed P3HT devices. We note however that the reduction factor for 1:2 DPPTT-T/$PC_{70}BM$ determined herein is significantly better than those observed for more

amorphous polymers such as PCDTBT or PTB7, that present reduction factors of 0.25 and 0.28 at $2.5 \times 10^{16}\ cm^{-3}$ respectively.[45] This illustrates how highly crystalline polymers and specifically those with low miscibility with fullerenes, have the advantage of reducing charge recombination losses, however at the expense of efficient exciton dissociation.

These results highlight the compromise between the presence of intermixed polymer/fullerene areas for optimal exciton dissociation and extended, relatively pure crystalline domains for efficient charge separation and slower recombination losses when using polymers as crystalline as DPPTT-T. Other studies of DPP-based OPV devices, have inversely correlated DPP polymer crystallite sizes with EQE values in the polymer-generating area.[4,7] In RR-P3HT, the situation is similar: while exciton dissociation is more efficient in intermixed as-spun blends compared to more crystallized, annealed blends,[46] non-geminate charge recombination is at least one order of magnitude slower in annealed vs. non-annealed devices.[44] In both cases, an efficient extraction of charges requires the existence of extended crystallised domains of polymer and fullerene to enable slow recombination kinetics; however, this comes at the expense of losing excitons that are generated far from the interface. As was shown in this study, exciton losses have a straightforward effect on EQE values and therefore in J_{SC}.

A challenge for the enhancement of the efficiency of DPP based devices is therefore the optimisation of blend morphology to enhance exciton separation efficiencies, whilst maintaining sufficient phase segregation to enable efficient charge collection. We note that one alternative strategy to address this compromise would be through increasing the polymer exciton diffusion length, thereby enabling more efficient exciton separation for the same blend morphology. In this regard, the rather short exciton lifetime of DPPTT-T, resulting from rapid non-radiative decay to ground, is a particular limitation of this polymer. Such rapid non-radiative losses may in part be associated, via the energy gap law, with its relative low

optical bandgap, although we note that many other factors influence non-radiative losses, and may be attractive targets to enhance the performance of this promising class of low-bandgap polymers.

Commented [DJR1]: Add reference to book or review paper here, and may be give some examples.

4. Conclusion

In this contribution we have related charge generation and charge recombination with blend microstructure and morphology for blends with different DPPTT-T/$PC_{70}BM$ ratios. We conclude that there is a critical trade-off between the optimum composition for exciton dissociation and for charge recombination slowing down, exemplifying the compromise between charge generation and transport in polymer/fullerene solar devices. The high crystallinity of DPPTT-T impedes an optimal intermixing with $PC_{70}BM$, resulting in intrinsic polymer exciton quenching limitations and formation of a relatively high amount of bound polaron pairs in the blends with low fullerene loadings. Although increasing the fullerene concentration helps to partially improve polymer exciton quenching, suppressing geminate recombination of bound polaron pairs and slowing down polaron non-geminate recombination, it also incurs in fullerene exciton decay losses. These intrinsic limitations are likely to result in EQE limitations for DPPTT-T. There is evidence that suggests that this might be also the case for others DPP-based devices, and that this could be related to high non-radiative losses in these low-bandgap polymers.

Experimental Section

Synthesis: polymer DPPTT-T was prepared according to the previously reported procedure.[10] Molecular weight and polydispersities (PDI) M_w = 35 kDa, M_n = 17 kDa, PDI = 2.06.

Film Preparation: 5 mg/mL DPPTT-T and 10 mg/mL $PC_{70}BM$ solutions in a mixture of 4:1 Chloroform to ODCB solvents were prepared and stirred overnight to prepare the films with the different $PC_{70}BM$ loadings, whose polymer to fullerene ratio were: 4 to 1 (20% $PC_{70}BM$),

2 to 1 (33% $PC_{70}BM$), 1 to 2 (67% $PC_{70}BM$) and 1 to 4 (80% $PC_{70}BM$). The films were spun on cleaned glass substrates for 1 minute at 2,500 rpms in air, and were then transferred into an inert-atmosphere glovebox until the measurements were performed. These films were used for UV-Vis, PL, sub-ps to µs-TAS and AFM. For XR-D samples, 10 mg/mL DPPTT-T and 20 mg/mL $PC_{70}BM$ solutions were used to prepare drop casted films with the appropriate concentrations ratio on cleaned glass substrates and dried overnight.

Device Preparation: active layers for devices were prepared in a similar fashion as for blends, except that the substrates had the electrodes deposited. Pre-cleaned, patterned indium tin oxide (ITO) substrates (15 Ω per square) were used. On top of the ITO substrates, PEDOT:PSS was spun at 3000 rpm and dried on a hot plate at 150°C in air for 20 minutes. The active layer was spun on top, in the same fashion as for the films and transferred to an inert-atmosphere glovebox. Following, the counter electrode of LiF (1 nm) and aluminum (100 nm) were deposited by vacuum evaporation at 3×10^{-7} mbar. The active area of the devices was 0.045 cm^2. All device characterization was performed in a sample chamber under inert conditions.

Steady-state UV-Visible and Photoluminescence (PL) spectroscopy: A Perkin Elmer Lambda 25 UV-vis spectrometer was used to obtain steady-state UV-Visible spectra from 300 to 1100 nm. Steady-state photoluminescence measurements were carried out in neat and blend films of DPPTT-T and $PC_{70}BM$ with a Fluorolog FM-32 spectrofluorometer using either a visible or an infrared detector depending on the fluorescence wavelengths detected. All the signals were corrected for absorbance at the excitation wavelength.

Transient absorption spectroscopy (TAS): TAS in the nanosecond and microsecond timescales was performed using a commercial optical parametric oscillator (Oppolette) pumped by a Nd:Yag laser to generate < 20 ns excitation pulses with 20 Hz repetition rate and

fluencies in the range of 5 to 25 μJ/cm^2 at 740 nm. Probe pulses with a time resolution of ~ 6 ns were generated using a 980 nm laser diode, operated by a laser-diode controller (ITC502, Thorlabs). The beam was focused onto the sample and then sent to a single grating monochromator, the detected using an InGaAs photodiode (Costronics Ltd.). Transient absorption decays were recorded with the aid of a LabView program referenced to a two-channel oscilloscope. The time resolution of this set-up was ~ 20 ns. Ultrafast transient absorption spectroscopy measurements were carried out with a commercial setup that comprises a 1 kHz Solstice (Newport Corporation) Ti:sapphire regenerative amplifier with 800 nm, 90 fs pulses. The output of this laser was split to generate the pump and probe pulses. The tunable pump pulse was generated in a TOPAS-Prime (Light conversion) optical parametric amplifier and used to excite the sample with energies between 5 and 25 μJ/cm^2 at 740 nm, with the fluencies adjusted to match the ns TAS measurements. The probe light was used to generate a Near-IR continuum (900-1450 nm) in a sapphire crystal. A HELIOS transient absorption spectrometer (Ultrafast Systems) was used for collecting transient absorption spectra and decays up to 6 ns. The time resolution of this set-up was 200 fs. The samples were kept at all times under a Nitrogen atmosphere.

Supporting Information
Supporting Information is available from the Wiley Online Library or from the author.

Acknowledgements
We gratefully acknowledge EPSRC (EP/IO1927B/1 and EP/K011987/1) for funding. ECF also thanks CONACyT (scholarship 309929) and the Kernahan Fund, Imperial College London for funding. The authors are also greatful with Prof. Jenny Nelson, Prof. Sophia Hayes and Michelle Vezie for fruitful discussions.

Received: ((will be filled in by the editorial staff))
Revised: ((will be filled in by the editorial staff))
Published online: ((will be filled in by the editorial staff))

[1] E. Zhou, S. Yamakawa, K. Tajima, C. Yang, K. Hashimoto, *Chem. Mater.* **2009**, *21*,

4055.

[2] J. C. Bijleveld, A. P. Zoombelt, S. G. J. Mathijssen, M. M. Wienk, M. Turbiez, D. M. De Leeuw, R. A. J. Janssen, *J. Am. Chem. Soc.* **2009**, *131*, 16616.

[3] W. Li, W. S. C. Roelofs, M. M. Wienk, R. a J. Janssen, *J. Am. Chem. Soc.* **2012**, *134*, 13787.

[4] W. Li, K. H. Hendriks, A. Furlan, W. S. C. Roelofs, M. M. Wienk, R. A. J. Janssen, *J. Am. Chem. Soc.* **2013**, *135*, 18942.

[5] W. Li, K. H. Hendriks, W. S. C. Roelofs, Y. Kim, M. M. Wienk, R. A. J. Janssen, *Adv. Mater.* **2013**, *25*, 3182.

[6] K. H. Hendriks, G. H. L. Heintges, V. S. Gevaerts, M. M. Wienk, R. A. J. Janssen, *Angew. Chemie - Int. Ed.* **2013**, *52*, 8341.

[7] W. Li, K. H. Hendriks, A. Furlan, W. S. C. Roelofs, S. C. J. Meskers, M. M. Wienk, R. A. J. Janssen, *Adv. Mater.* **2014**, *26*, 1565.

[8] W. Li, K. H. Hendriks, M. M. Wienk, R. A. J. Janssen, *Acc. Chem. Res.* **2016**, *49*, 78.

[9] L. Ye, S. Zhang, W. Ma, B. Fan, X. Guo, Y. Huang, H. Ade, J. Hou, *Adv. Mater.* **2012**, *24*, 6335.

[10] H. Bronstein, Z. Chen, R. S. Ashraf, W. Zhang, J. Du, J. R. Durrant, P. S. Tuladhar, K. Song, S. E. Watkins, Y. Geerts, M. M. Wienk, R. A. J. Janssen, T. Anthopoulos, H. Sirringhaus, M. Heeney, I. McCulloch, *J. Am. Chem. Soc.* **2011**, *133*, 3272.

[11] X. Zhang, L. J. Richter, D. M. Delongchamp, R. J. Kline, M. R. Hammond, I. McCulloch, M. Heeney, R. S. Ashraf, J. N. Smith, T. D. Anthopoulos, B. Schroeder, Y. H. Geerts, D. A. Fischer, M. F. Toney, *J. Am. Chem. Soc.* **2011**, *133*, 15073.

[12] H. Bronstein, E. Collado-Fregoso, A. Hadipour, Y. W. Soon, Z. Huang, S. D. Dimitrov, R. S. Ashraf, B. P. Rand, S. E. Watkins, P. S. Tuladhar, I. Meager, J. R. Durrant, I. McCulloch, *Adv. Funct. Mater.* **2013**, *23*, 5647.

[13] I. Meager, R. S. Ashraf, S. Mollinger, B. C. Schroeder, H. Bronstein, D. Beatrup, M. S.

Vezie, T. Kirchartz, A. Salleo, J. Nelson, I. McCulloch, *J. Am. Chem. Soc.* **2013**, *135*, 11537.

[14] C. B. Nielsen, M. Turbiez, I. McCulloch, *Adv. Mater.* **2013**, *25*, 1859.

[15] R. S. Ashraf, I. Meager, M. Nikolka, M. Kirkus, M. Planells, B. C. Schroeder, S. Holliday, M. Hurhangee, C. B. Nielsen, H. Sirringhaus, I. McCulloch, *J. Am. Chem. Soc.* **2015**, *137*, 1314.

[16] S. Albert-Seifried, D.-H. Ko, S. Hüttner, C. Kanimozhi, S. Patil, R. H. Friend, *Phys. Chem. Chem. Phys.* **2014**, *16*, 6743.

[17] K. H. Kim, S. Park, H. Yu, H. Kang, I. Song, J. H. Oh, B. J. Kim, *Chem. Mater.* **2014**, *26*, 6963.

[18] S. Venkatesan, N. Adhikari, J. Chen, E. C. Ngo, A. Dubey, D. W. Galipeau, Q. Qiao, *Nanoscale* **2014**, 1011.

[19] C. J. Mueller, M. Brendel, P. Ruckdeschel, J. Pflaum, M. Thelakkat, *Adv. Energy Mater.* **2015**, 1.

[20] M. S. Vezie, S. Few, I. Meager, G. Pieridou, B. Dörling, R. S. Ashraf, A. R. Goñi, H. Bronstein, I. Mcculloch, S. C. Hayes, M. Campoy-Quiles, J. Nelson, *Nat. Mater.* **2016**, *15*, DOI: 10.1038/NMAT4645.

[21] M. M. Wienk, M. Turbiez, J. Gilot, R. a. J. Janssen, *Adv. Mater.* **2008**, *20*, 2556.

[22] C. Kästner, D. a. M. Egbe, H. Hoppe, *J. Mater. Chem. A* **2015**, *3*, 395.

[23] F. C. Jamieson, E. B. Domingo, T. McCarthy-Ward, M. Heeney, N. Stingelin, J. R. Durrant, *Chem. Sci.* **2012**, *3*, 485.

[24] E. Collado-Fregoso, P. Bou, Z. Fei, E. Gann, S. Ashraf, Z. Li, C. R. Mcneill, J. R. Durrant, M. Heeney, *Chem. Mater.* **2015**, *27*, 7934.

[25] A. J. Lewis, A. Ruseckas, O. P. M. Gaudin, G. R. Webster, P. L. Burn, I. D. W. Samuel, *Org. Electron. physics, Mater. Appl.* **2006**, *7*, 452.

[26] S. Dimitrov, B. Schroeder, C. Nielsen, H. Bronstein, Z. Fei, I. McCulloch, M. Heeney,

J. Durrant, *Polymers (Basel)*. **2016**, *8*, 14.

[27] S. Cook, A. Furube, R. Katoh, L. Han, *Chem. Phys. Lett.* **2009**, *478*, 33.

[28] S. D. Dimitrov, Z. Huang, F. Deledalle, C. B. Nielsen, B. C. Schroeder, R. S. Ashraf, S. Shoaee, I. McCulloch, J. R. Durrant, *Energy Environ. Sci.* **2014**, *7*, 1037.

[29] S. D. Dimitrov, C. B. Nielsen, S. Shoaee, P. S. Tuladhar, J. Du, I. Mcculloch, J. R. Durrant, *J. Phys. Chem. Lett.* **2011**, *3*, 140.

[30] Z. Huang, E. C. Fregoso, S. Dimitrov, P. S. Tuladhar, Y. W. Soon, H. Bronstein, I. Meager, W. Zhang, I. McCulloch, J. R. Durrant, *J. Mater. Chem. A* **2014**, *2*, 19282.

[31] F. Piersimoni, S. Chambon, K. Vandewal, R. Mens, T. Boonen, A. Gadisa, M. Izquierdo, S. Filippone, B. Ruttens, J. D'haen, N. Martin, L. Lutsen, D. Vanderzande, P. Adriaensens, J. V. Manca, *J. Phys. Chem. C* **2011**, *115*, 10873.

[32] J. R. Tumbleston, L. Yang, W. You, H. Ade, *Polym. (United Kingdom)* **2014**, *55*, 4884.

[33] G. Lanzani, *The Photophysics behind Photovoltaics and Photonics*; Wiley-VCH: Weinheim, Germany, **2012**.

[34] A. Köhler, H. Bässler, *Electronic Processes in Organic Semiconductors*; Wiley-VCH: Weinheim, Germany, **2015**.

[35] T. M. Clarke, A. M. Ballantyne, S. Tierney, M. Heeney, W. Duffy, I. Mcculloch, J. Nelson, J. R. Durrant, *J. Phys. Chem. C* **2010**, *114*, 8068.

[36] A. Baumann, T. J. Savenije, D. H. K. Murthy, M. Heeney, V. Dyakonov, C. Deibel, *Adv. Funct. Mater.* **2011**, *21*, 1687.

[37] G. Grancini, N. Martino, M. R. Antognazza, M. Celebrano, H. Egelhaaf, G. Lanzani, *J. Phys. Chem. C* **2012**, *116*, 9838.

[38] S. A. Hawks, F. Deledalle, J. Yao, D. G. Rebois, G. Li, J. Nelson, Y. Yang, T. Kirchartz, J. R. Durrant, *Adv. Energy Mater.* **2013**, *3*, 1201.

[39] M. Scarongella, J. De Jonghe-Risse, E. Buchaca-Domingo, M. Causa, Z. Fei, M. Heeney, J. E. Moser, N. Stingelin, N. Banerji, *J. Am. Chem. Soc.* **2015**, *137*, 2908.

[40] D. W. Gehrig, I. A. Howard, S. Sweetnam, T. M. Burke, M. D. Mcgehee, F. Laquai, *Macromol. Rapid Commun.* **2015**.

[41] S. Foster, F. Deledalle, A. Mitani, T. Kimura, K. B. Kim, T. Okachi, T. Kirchartz, J. Oguma, K. Miyake, J. R. Durrant, S. Doi, J. Nelson, *Adv. Energy Mater.* **2014**, *4*, 1.

[42] C. M. Proctor, M. Kuik, T. Nguyen, *Prog. Polym. Sci.* **2013**, *38*, 1941.

[43] F. Zhang, O. Inganäs, Y. Zhou, K. Vandewal, *Natl. Sci. Rev.* **2016**, *doi: 10.10*.

[44] R. Hamilton, C. G. Shuttle, B. O'Regan, T. C. Hammant, J. Nelson, J. R. Durrant, *J. Phys. Chem. Lett.* **2010**, *1*, 1432.

[45] F. Deledalle, *PhD Thesis*, November, **2013**.

[46] P. E. Keivanidis, T. M. Clarke, S. Lilliu, T. Agostinelli, J. E. MacDonald, J. R. Durrant, D. D. C. Bradley, J. Nelson, *J. Phys. Chem. Lett.* **2010**, *1*, 734.

[47] C. Cabanetos, A. El Labban, J. A. Bartelt, J. D. Douglas, W. R. Mateker, J. M. J. Frechet, M. D. McGehee, P. M. Beaujuge, *J. Am. Chem. Soc.* **2013**, *135*, 4656.

[48] C. Cui, W.-Y. Wong, Y. Li, *Energy Environ. Sci.* **2014**, *7*, 2276.

[49] Z. He, C. Zhong, X. Huang, W. Y. Wong, H. Wu, L. Chen, S. Su, Y. Cao, *Adv. Mater.* **2011**, *23*, 4636.

[50] C. Liu, C. Yi, K. Wang, Y. Yang, R. S. Bhatta, M. Tsige, S. Xiao, X. Gong, *ACS Appl. Mater. Interfaces* **2015**, *7*, 4928.

[51] Y. Huang, X. Guo, F. Liu, L. Huo, Y. Chen, T. P. Russell, C. C. Han, Y. Li, J. Hou, *Adv. Mater.* **2012**, *24*, 3383.

[52] L. Ye, S. Zhang, W. Zhao, H. Yao, J. Hou, *Chem. Mater.* **2014**, *26*, 3603.

[53] H. C. Chen, Y. H. Chen, C. C. Liu, Y. C. Chien, S. W. Chou, P. T. Chou, *Chem. Mater.* **2012**, *24*, 4766.

[54] J. D. A. Lin, O. V. Mikhnenko, J. Chen, Z. Masri, A. Ruseckas, A. Mikhailovsky, R. P. Raab, J. Liu, P. W. M. Blom, M. A. Loi, C. J. García-Cervera, I. D. W. Samuel, T.-Q. Nguyen, *Mater. Horizons* **2014**, *1*, 280.

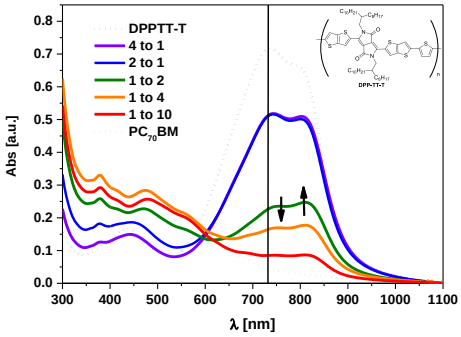

Figure 1. Steady state UV-vis absorption of neat and blend films of DPPTT-T and $PC_{70}BM$ with different polymer to $PC_{70}BM$ weight ratios. The blend films have thicknesses varying between 110 and 150 nm.

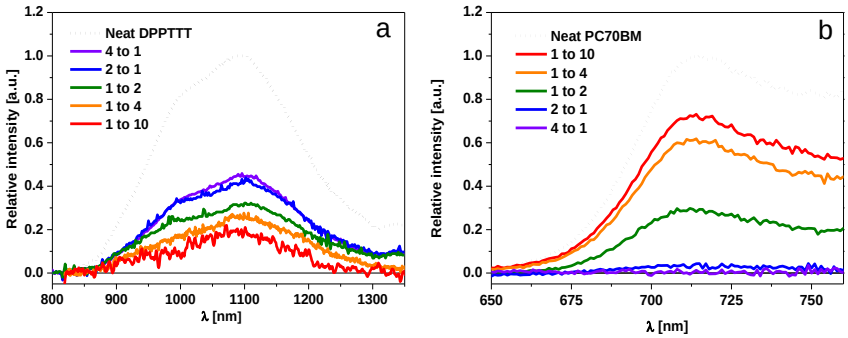

Figure 2. a) Steady state PLQ studies of DPPTT-T as a function of $PC_{70}BM$ loading, exciting at 740 nm b) steady state PLQ studies of $PC_{70}BM$ as a function of DPPTT-T loading for the same blend films, exciting at 520 nm, where DPPTT-T has a minimum absorption. PL data was normalized for photon film absorption at the excitation wavelength and then normalized to the neat maximum.

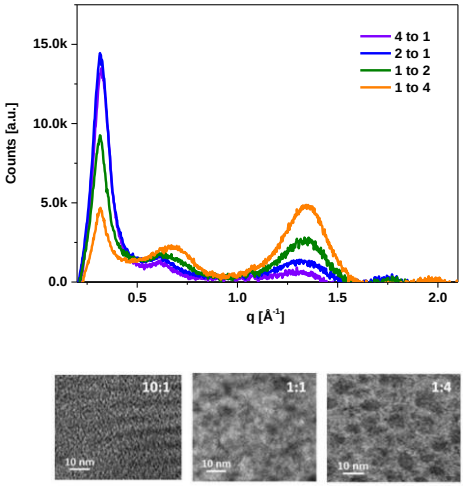

Figure 3. Top: Wide-angle X-ray diffraction (WAXD) patterns for the different DPPTT-T/$PC_{70}BM$ blends. Data was corrected with a factor that accounts for the differences in film thickness. Bottom: TEM micrographs for 10:1, 1:1 and 1:4 DPPTT-T/$PC_{70}BM$ blends, showing the formation of $PC_{70}BM$-rich areas as the fullerene concentration is increased.

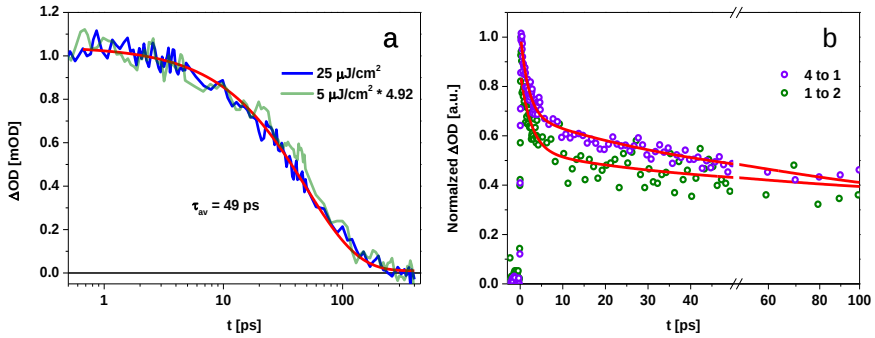

Figure 4. a) Neat DPPTT-T kinetics, after excitation at 740 nm, and averaged probe between 990 and 1010 nm at 5 and 25 µJ/cm^2, data at 25 µJ/cm^2 was rescaled. Data at 5 µJ/cm^2 have a decay time $\tau = 58 \pm 7$ ps, thus within the error margin of the decay at 25 µJ/cm^2. The data was corrected for polymer absorption at the excitation wavelength. b) Normalized sub-ps transient absorption exciton dynamics exciting at 740 nm with 25 µJ/cm^2, probed at 1300 nm for 4 to 1 and 1 to 2 blend films. The decays were fitted to a biexponential function plus a constant term (see text).

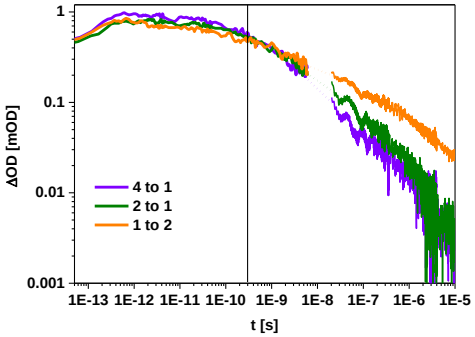

Figure 5. Sub-ps to µs transient absorption dynamics of the different blend films, after excitation at 740 nm at 5 µJ/cm^2 and probed at 980 nm, showing similar polaron yields per quenched exciton, but slower recombination as the fullerene concentration is increased.

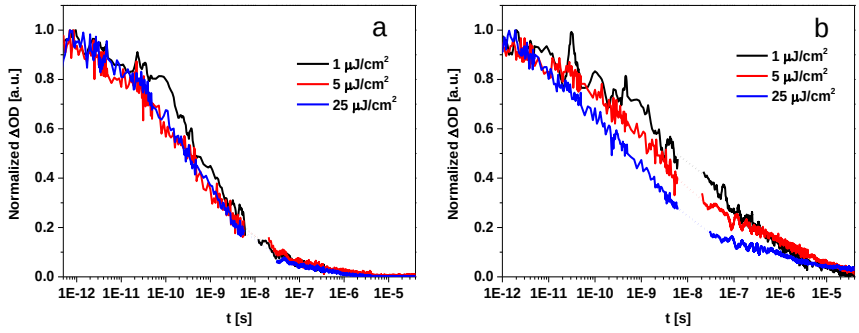

Figure 6. Normalized sub-ps to µs transient absorption recombination dynamics pumping at 740 nm and probing at 980 nm and as a function of excitation intensity for a) 4:1 and b) 1:4 blend film.

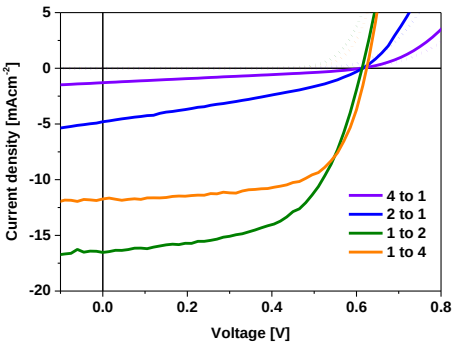

Figure 7. *J-V* curves for the best devices fabricated with different DPPTT-T:$PC_{70}BM$ ratios, measured under constant illumination with 100 $mWcm^{-2}$, AM1.5 spectrum from a solar simulated light at room temperature. Dotted lines correspond to dark current of the respective cells. Devices have a standard architecture: ITO/PEDOT:PSS/Active blend/LiF/Al.

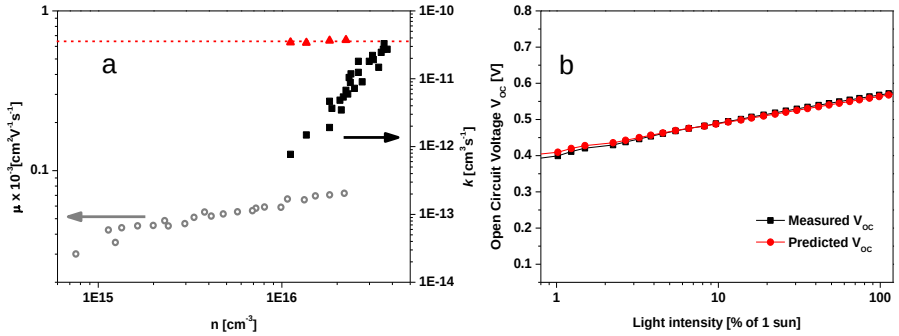

Figure 8. a) Average carrier mobilities (left axis) and effective non-geminate recombination constant (right axis) as a function of charge density for the optimal, 1:2 DPPTT-T/$PC_{70}BM$ device, in red triangles the Langevin recombination rate constant is shown. b) V_{OC} reconstruction for a range of light intensities for the same device.

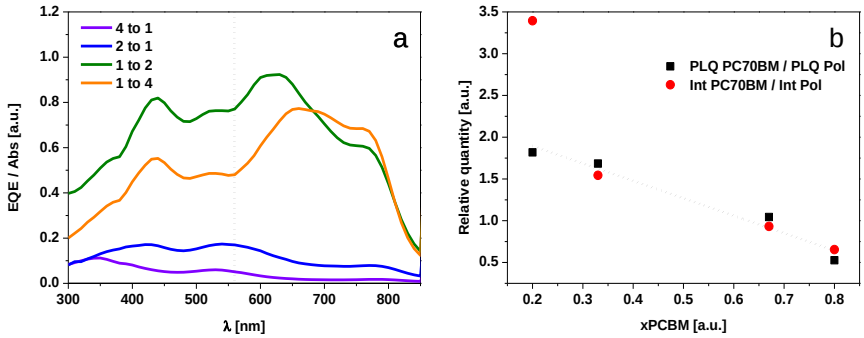

Figure 9. a) EQE/Abs for devices fabricated with 4 to 1, 2 to 1, 1 to 2 and 1 to 4 DPPTT-T:$PC_{70}BM$ ratios. The dotted line divides the areas considered for the integration in b), see text. b) $PC_{70}BM$ PLQ divided by DPPTT-T PLQ (black squares) and integrated EQE/Abs in the $PC_{70}BM$ area (Int $PC_{70}BM$) divided by integrated EQE/Abs in the polymer area (red circles) as a function of the fraction amount of $PC_{70}BM$, see text for more details on this relative quantities.

Table 1. Photovoltaic properties of best DPP-based and some of the best current non-DPP based devices with standard architectures (ITO/PEDOT:PSS/Active blend/Ca (or LiF)/Al) with similar thicknesses and with $PC_{70}BM$ as acceptor.

Polymer	J_{SC} (mA/cm^2)	V_{OC} (V)	*FF*	EQE_{max} (Polymer)	EQE_{max} ($PC_{70}BM$)	%PCE	Thickness (nm)	Band-gap (eV)
DPP-based best performing conventional devices (increasing J_{sc})								
PDPPTPT[6]	14	0.80	0.67	0.58	0.52	7.4	115	1.82
PDPP3T[6]	15.4	0.67	0.69	0.49	0.51	7.1	134	1.56
PDPP3T*alt*TPT[6]	15.9	0.75	0.67	0.59	0.57	8.0	110	-
PDPP4T[4]	16.0	0.64	0.69	0.6	0.55	7.1	115	1.45
PBDTT-SeDPP[17]	16.8	0.69	0.62	0.53	0.54	7.0	100	1.55
DPPTT-TC2[13]	18.6	0.61	0.64	0.61	0.69	7.3	115	1.4[a)]
DPPTT-TC3[15]	19.0	0.59	0.62	0.61	0.78	7.0	115	1.4[a)]
Average	**16.5**	**0.68**	**0.66**	**0.57**	**0.59**	**7.3**	**115**	**1.53**
Some of the best performing non-DPP-based conventional devices (increasing J_{sc})								
PBDTTPD[47] (2EH/C7)	12.6	0.97	0.7	0.73	0.64	8.5	110	-
PBDTT-S-TT[48]	15.3	0.84	0.66	0.70	0.60	8.4	95	2.14
PTB7[49,50]	15.75	0.76	0.7	0.75	0.71	8.4	90	1.68[a)]
PBDTDTTT-S-T[51]	16.35	0.69	0.66	0.73	0.51	7.8	110	1.47
PBDT-TS1[52]	17.4	0.80	0.66	0.72	0.71	9.2	100	1.81
PBDT-TFQ[53]	17.9	0.76	0.58	0.8	0.85	8	106	1.73[a]
PTB7-D1[50]	19.6	0.79	0.65	0.85	0.82	10.1	100	1.75
Average	**16.4**	**0.80**	**0.66**	**0.75**	**0.69**	**8.6**	**102**	**1.76**

[a)]Optical bandgap, estimated from the onset of UV−vis spectrum of the film. Otherwise determined by cyclic voltammetry measurements.

Table 2. Photoluminescence quenching values obtained from Figure 1, and the corresponding DPPTT-T and $PC_{70}BM$ domain sizes.

Blend	% PLQ Polymer	% PLQ $PC_{70}BM$	Average PLQ $PC_{70}BM$ domain size (nm)[a)]	Average TEM $PC_{70}BM$ domain size (nm)[b)]
4:1	55	100	< 2.0	< 2.0
2:1	57	96	2.0	-
1:1	-	-	-	4.8
1:2	68	71	5.4	-
1:4	74	39	7.8	8.0
1:10	81	28	8.4	-

[a)]Obtained using the equation $L = L_{ex}(1 - PLQ)^{1/2}$, where L is the distance that the exciton travels before it reaches an interface, and L_{ex} is the exciton diffusion length. Here, the domain sizes are estimated as an approximate circumference diameter of size $2L$.
[b)]Estimated from average visual measurements of the smallest diameter of dark areas in the TEM micrographs.

Table 3. Comparison between the polymer PLQ values as obtained from steady-state PL and %QE as obtained from ultrafast TAS. $\%QE$ is calculated using: $\%QE = [A_2/(A_1 + A_2)] \times 100$

Blend	% PLQ Polymer	$\tau_1[ps](A_1)$	$\tau_2[ps](A_2)$	$\%QE$
4 to 1	55	52 (0.32)	1.9 (0.34)	52
2 to 1	57	44 (0.23)	2.0 (0.35)	60
1 to 2	68	46 (0.16)	2.6 (0.32)	66
1 to 4	74	-	-	-

Table 4. Photovoltaic parameters for the corresponding devices shown in Figure 7

	4 to 1	2 to 1	1 to 2	1 to 4
J_{SC} (mAcm^{-2})	1.30	4.80	16.53	11.73
V_{OC} (V)	0.61	0.61	0.61	0.62
Fill Factor	0.29	0.33	0.58	0.65
PCE (%)	0.23	0.97	5.87	4.77

Keywords: organic photovoltaics, DPP-based solar cells, donor-acceptor composition, EQE limitations

Elisa Collado-Fregoso, Florent Deledalle, Hendrik Utzat, Pabitra S. Tuladhar, Stoichko D. Dimitrov, Alexander Gillett, Ching-Hong Tan, Weimin Zhang, Iain McCulloch and James R. Durrant*

Photophysical study of DPPTT-T/$PC_{70}BM$ blends and solar devices as a function of fullerene loading: an insight into EQE limitations of DPP-based polymers.

ToC figure ((Please choose one size: 55 mm broad × 50 mm high **or** 110 mm broad × 20 mm high. Please do not use any other dimensions))